Journal of Materials Science: Materials in Energy

CORRESPONDENCE Open Access

Effect of reduced graphene oxide addition on corrosion resistance and magnetic properties of sintered NdFeB magnets

J. C. Silva-Filho[1,4*], S. C. Silva[2], H. Takiishi[3], T. Mazon[4], E. C. Venancio[1], R. C. C. Rangel[1], I. Y. Abe[2], S. R. Janasi[3], M. A. Meira[5], S. A. Romero[5], T. F. Silva[5], C. L. Rodrigues[5], S. Guimaraes[6], B. Freelon[7], R. A. Antunes[1], L. G. Martinez[3], M. T. Escote[1] and J. F. Q. Rey[1]

Abstract
Neodymium–Iron–Boron (NdFeB) permanent magnets are indispensable in energy technologies such as wind turbines, electric vehicles, and robotics, but their processing is hindered by spontaneous powder ignition and severe corrosion susceptibility. Here, we demonstrate that incorporating 0.02 wt% reduced graphene oxide (rGO) during mechanical milling enables safe powder handling in ambient conditions without inert atmospheres, while simultaneously enhancing functional performance. Milling time was found to be critical: at 30 min, sintered magnets achieved remanence of 1.11 T, coercivity of 794 kA·m^{-1}, and a maximum energy product of 242 kJ·m^{-3}, values comparable to commercial N35 magnets without heavy rare-earth additions. Electrochemical impedance spectroscopy revealed corrosion resistance up to two orders of magnitude higher than values typically reported for coated NdFeB magnets. Structural, electrochemical, and depth-profiling analyses confirmed that rGO acts as both a solid lubricant and encapsulating barrier, balancing grain refinement, oxidation suppression, and interfacial stabilization. This work establishes rGO-assisted processing as a scalable, sustainable, and cost-effective pathway to high-performance NdFeB magnets for next-generation energy conversion and storage systems.

Keywords NdFeB permanent magnets, Reduced graphene oxide, Mechanical milling, Corrosion resistance, Magnetic properties, Powder metallurgy

1 Introduction

Neodymium–Iron–Boron (NdFeB) permanent magnets are widely recognized as the third generation of rare-earth magnetic materials and are indispensable to the energy transition. Their high remanence (Br), coercivity (iHc), and maximum energy product (BH_{max}) make them key components in wind turbines, electric and hybrid vehicles, robotics, and compact consumer electronics [1, 2]. The strategic role of these magnets extends to aerospace, telecommunications, and defense technologies, reinforcing their importance for economic and technological sovereignty [3]. As global demand grows, supply

*Correspondence:
J. C. Silva-Filho
jorgecsilvaf@gmail.com
[1]Federal University of ABC, Santo André, Brazil
[2]University of São Paulo, São Paulo, Brazil
[3]Nuclear and Energy Research Institute, São Paulo, Brazil
[4]Centro de Tecnologia da Informação Renato Archer, Campinas, São Paulo, Brazil
[5]Institute of Physics, São Paulo, Brazil
[6]Aeronautical Technology Institute, São José dos Campos, São Paulo, Brazil
[7]Department of Physics, Texas Center for Superconductivity, University of Houston, Houston, TX, USA

chain vulnerabilities and sustainability concerns intensify, requiring advances in both processing and performance [4].

NdFeB magnets are known for their exceptional magnetic properties, but they exhibit a marked sensitivity to oxidation, originating from the rare-earth-rich phases present in their microstructure. During mechanical milling, particles can spontaneously ignite upon exposure to air, demanding glove boxes or inert atmospheres for safe handling [5]. Oxidation promotes the formation of Nd_2O_3 and porosity, reducing densification during sintering and compromising magnetic coupling between grains [6]. Even trace impurities of carbon and oxygen can alter coercivity and introduce microstructural defects that degrade magnetic stability [7, 8]. In service, NdFeB magnets are highly vulnerable to corrosion in humid or chloride-rich environments, with corrosion rates surpassing those of conventional ferrous alloys [3, 4]. This dual challenge of safe processing and environmental degradation remains a critical barrier to wider adoption in high-performance sectors.

Conventional mitigation strategies include alloying and surface modification. Alloying with heavy rare-earth elements such as dysprosium (Dy) and terbium (Tb) increases coercivity and thermal stability but raises costs and accentuates supply risks, as these elements are scarce and geographically concentrated [9, 10]. Surface coatings, including phosphate passivation, nickel phosphorus layers, or diamond-like carbon films, can reduce corrosion but are prone to delamination and mechanical failure, especially under thermal or mechanical stress [11, 12]. Recycling approaches, including hydrogen decrepitation, also face limitations due to reoxidation during powder reprocessing [13]. As such, there is a need for multifunctional solutions that simultaneously improve processing safety, structural integrity, and environmental stability, while avoiding cost escalation.

Graphene derivatives, particularly reduced graphene oxide (rGO), offer a promising pathway. rGO combines high specific surface area, chemical stability, and nearly impermeable layered structures with functional groups that can interact with metallic surfaces [14]. Previous studies have demonstrated that GO/rGO coatings enhance corrosion resistance of NdFeB magnets by up to two orders of magnitude and improve hardness and wear resistance [15]. rGO may also function as a solid lubricant during milling, preventing cold welding and agglomeration, while facilitating homogeneous dispersion of phases [16]. Its barrier effect against oxygen diffusion and its stability at elevated temperatures further support its use in powder metallurgy of rare-earth magnets [13, 17]. However, most prior work has focused on external coatings applied after sintering, while little attention has been given to the direct incorporation of rGO during powder processing. Furthermore, the combined effect of milling time and rGO dispersion on microstructural evolution, surface chemistry, and final magnetic properties is still poorly understood [13, 16].

This study addresses these gaps by systematically investigating the incorporation of rGO during mechanical milling of NdFeB powders and its influence on sintered magnets. Four composites containing 0.02 wt% rGO were prepared with milling times ranging from 7 to 45 min. Characterizations included XRD, Raman, TEM, XPS, RBS, and MEV, coupled with magnetic measurements and electrochemical impedance spectroscopy.

2 Materials and methods

Reduced graphene oxide (rGO) was synthesized following the thermal reduction route described by Silva Filho et al. (2020) [16]. Graphene oxide (GO) was first obtained through a modified Hummers method, producing few-layered nanosheets with abundant oxygen-containing functional groups. The reduction step was carried out under controlled heating, partially restoring the sp^2 network while preserving residual oxygen groups that contribute to surface reactivity and dispersion capacity. This synthesis route has been previously validated as efficient for obtaining stable rGO structures suitable for integration with metallic powders [15, 17].

Commercial NdFeB alloy ingots with nominal composition $Nd_{30.21}Pr_{0.64}Fe_{63.64}B_{0.94}Co_{2.93}Dy_{1.05}Cu_{0.15}Al_{0.15}Ga_{0.21}$ (wt%) were selected as the base material. This alloy represents a typical formulation used in high-performance magnets [6, 16]. Prior to milling, the ingots were pretreated by hydrogen decrepitation to obtain a friable microstructure suitable for powder processing, in accordance with established protocols for NdFeB [10]. For each batch, 15 g of alloy were subjected to mechanical milling with 0.02 wt% rGO, a content previously optimized for dispersion in metallic matrices within a compositional range of 0.02–0.10 wt% [13, 18]. Fixing the rGO content at 0.02 wt% allows the effect of milling time on powder handling safety, microstructural evolution, corrosion resistance, and magnetic properties to be isolated. Milling times of 7, 15, 30, and 45 min were employed to produce four distinct NdFeB–rGO composites. The resulting powders were compacted and consolidated by conventional powder metallurgy routes, following procedures detailed in Filho et al. (2024) [18].

The powder samples were designated as NdFeB–rGO–1, NdFeB–rGO–2, NdFeB–rGO–3, and NdFeB–rGO–4, corresponding to 7, 15, 30, and 45 min of milling time, respectively. After sintering, the samples were renamed Magnet–1 to Magnet–4, as detailed in Table 1. This systematic nomenclature was adopted to facilitate correlation between milling conditions, structural features, and functional properties.

Table 1 Identification of NdFeB–rGO composite powders and corresponding sintered magnets as a function of milling time. NdFeB–rGO–1 to –4 denote composite powders milled for 7, 15, 30, and 45 min, respectively

Composite powder	After sintering	Milling time (min)
NdFeB-rGO-1	Magnet-1	7
NdFeB-rGO-2	Magnet-2	15
NdFeB-rGO-3	Magnet-3	30
NdFeB-rGO-4	Magnet-4	45

After sintering, the corresponding magnets are labeled Magnet-1 to Magnet-4

2.1 Characterization

Characterization techniques were employed to evaluate structural, morphological, surface, and functional properties of both powders and sintered magnets. X-ray diffraction (XRD) was performed to identify crystalline phases and estimate crystallite size via the Scherrer equation [19, 20]. Raman spectroscopy was used to probe carbon-related disorder and graphitic domains, providing information on the presence and structural quality of rGO in the composites [17]. Transmission electron microscopy (TEM) allowed direct observation of particle morphology and rGO distribution, complementing XRD results with nanoscale structural details.

Surface chemical states were investigated by X-ray photoelectron spectroscopy (XPS), which enabled analysis of carbon, oxygen, and metallic bonding environments. This method has proven particularly effective in evaluating rGO functionalization and its interactions with metallic matrices [21]. To extend chemical analysis to depth profiling, Rutherford Backscattering Spectrometry (RBS) and Elastic Backscattering Spectrometry (EBS) were employed using a ^{4}He ion beam. Spectra were simulated and fitted using SIMNRA 7 [22] and MultiSIMNRA [23], enabling accurate quantification of elemental gradients across the magnet surface.

Magnetic properties were measured using a permeameter to obtain demagnetization curves and extract Br, iHc, and BHmax values. These parameters were used to assess the influence of milling time and rGO on the intrinsic performance of the magnets, in line with previous studies of NdFeB processing [24, 25]. Electrochemical impedance spectroscopy (EIS) was performed in 3.5 wt% NaCl solution, adopting a three-electrode setup, to quantify corrosion resistance. This test configuration is widely accepted for benchmarking the corrosion behavior of NdFeB alloys [26, 27]. Open circuit potential (OCP) was monitored prior to EIS measurements to ensure stabilization of the electrochemical system. Also, scanning electron microscopy (MEV/FESEM) was used to analyze grain morphology and microstructural evolution after sintering. Also, the conditions and parameters of the characterizations and equipment are described in Supplementary Information (S1). All samples corresponding to each milling condition were independently prepared in triplicate following the same powder metallurgy route. The reproducibility of the results was confirmed by the consistency of microstructural, magnetic, and electrochemical trends across these independently prepared batches.

3 Results and discussion

3.1 Characterization of GO and rGO

The structural and vibrational analyses of graphene oxide (GO) and reduced graphene oxide (rGO) provided insights into their transformation and suitability as additives for NdFeB powders. Figure 1a shows the XRD patterns of both materials. GO displayed a sharp reflection at $2\theta \approx 12°$, corresponding to the (001) plane, which is associated with increased interlayer spacing caused by oxygen-containing groups and intercalated water molecules [18]. After thermal reduction, the diffraction peak shifted to $2\theta \approx 25°$, consistent with the partial restoration of the graphitic structure and significant removal of oxygenated groups [28]. This shift demonstrates the effectiveness of the adopted thermal reduction process, as previously reported for rGO obtained under similar conditions [29].

Raman spectroscopy further confirmed structural changes during reduction (Fig. 1b). The GO spectrum exhibited two main bands: the D band (~ 1347 cm^{-1}), attributed to disordered sp^3 carbon domains, and the G band (~ 1593 cm^{-1}), related to in-plane vibration of sp^2 carbon atoms. After reduction, rGO maintained the characteristic D and G bands with altered intensity ratios. No well-defined 2D band was observed in either GO or rGO. Instead, a broad and weak feature appeared in the higher wavenumber region, typically associated with second-order carbon bands, as commonly reported for thermally reduced graphene oxide. The slight variations in intensity and noise level between GO and rGO are attributed to partial restoration of sp^2 domains and increased structural disorder after thermal reduction, rather than to the formation of a distinct 2D band [15].

To complement structural analysis (Fig. 1c), X-ray photoelectron spectroscopy (XPS) was employed to probe surface chemistry. The C 1s spectrum of GO showed peaks corresponding to sp^2-hybridized carbon (C = C) at ~ 284.8 eV, hydroxyl groups at ~ 286.2 eV, and carboxyl/epoxy contributions at ~ 289.6 eV. After reduction, the C 1s spectrum of rGO revealed increased sp^2 character but also persistent sp^3 and C = O contributions, confirming incomplete removal of oxygen functionalities [28]. The O 1s spectrum reinforced this trend, with residual carbonyl and ether groups still present. These results demonstrate that the thermal method did not produce fully graphitic carbon but retained functional moieties that may enhance interfacial interactions with metallic particles.

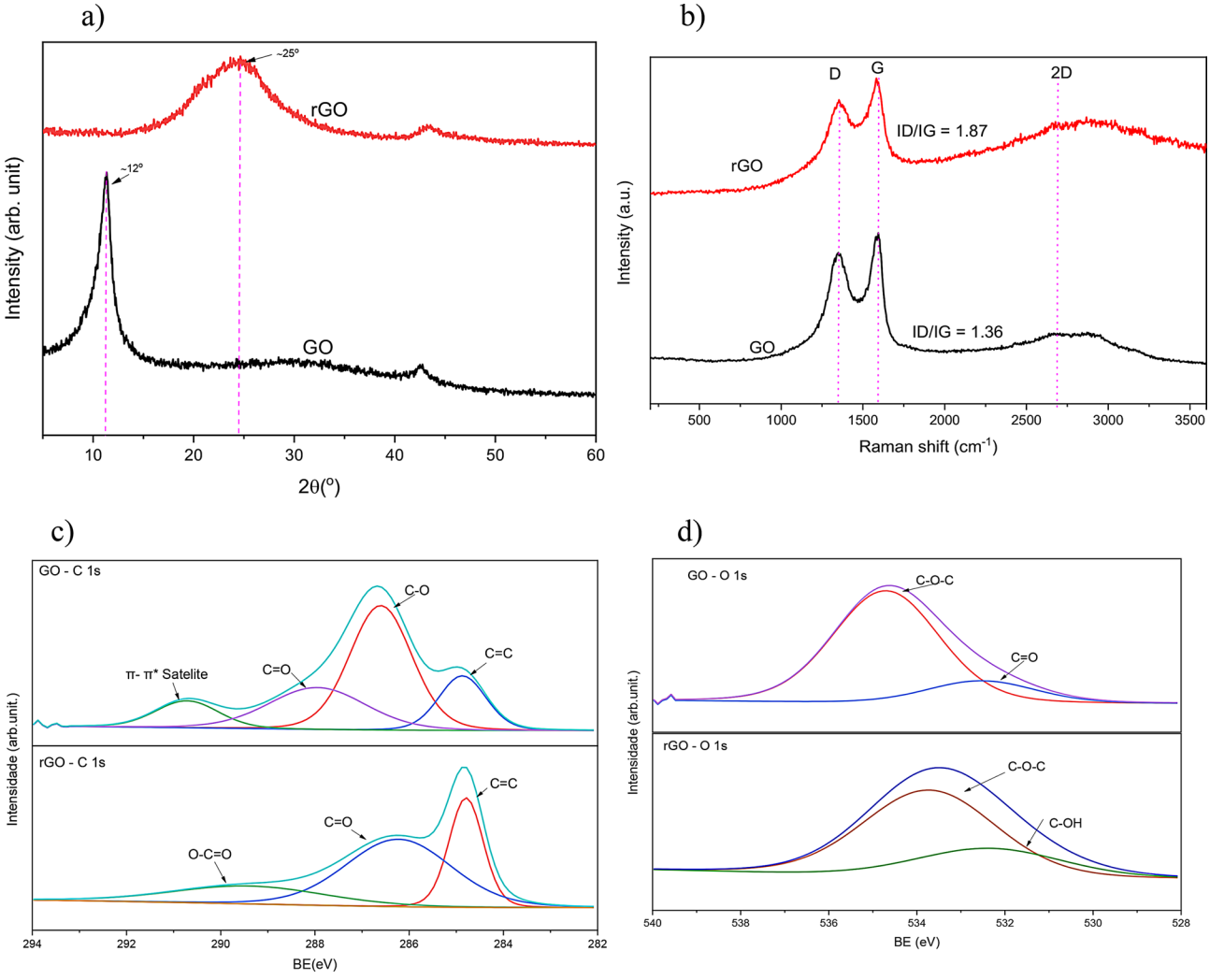

Fig. 1 Structural and chemical characterization of GO and rGO: (**a**) XRD patterns showing the shift of the (001) peak from 12° in GO to 25° in rGO; (**b**) Raman spectra showing the characteristic D and G bands and a weak second-order feature at higher wavenumbers, consistent with partially reduced graphene oxide; (**c**) XPS C 1s deconvolution, showing increased sp^2 contributions after reduction; (**d**) XPS O 1s deconvolution, revealing residual oxygenated groups

Also, a brief description of the NdFeB–rGO composites by XPS is expressed in SI 2.

Such residual oxygen groups are relevant in the context of powder metallurgy because they promote chemical compatibility between rGO sheets and NdFeB alloy surfaces. Previous reports emphasized that partially reduced graphene oxide often performs better than fully reduced graphene in composite systems, due to its ability to anchor on metallic matrices, thereby assuring interfacial compatibility while still maintaining barrier properties [30, 31]. In this work, the balance between restored graphitic domains (providing conductivity and barrier effects) and residual oxygen groups (providing bonding functionality) is expected to be advantageous for NdFeB–rGO composites.

XPS analysis shows that the rGO used in this study retains a significant fraction of oxygen-containing functional groups while partially restoring sp^2 carbon domains. Specifically, the C 1s spectrum indicates an sp^2 carbon contribution of approximately 40–45 at% together with residual oxygenated species (C–O and C = O) accounting for ~ 20–25 at%, as detailed in the SI. This chemical configuration enables simultaneous barrier effects associated with graphitic regions and interfacial bonding through oxygen functionalities, which is particularly beneficial for stabilizing the NdFeB–rGO interface.

The XRD and Raman results obtained here corroborate earlier reports describing the typical structural signatures of thermally reduced GO. For instance, Silva Filho et al. (2020) demonstrated that their method produced rGO with interlayer spacing close to 0.34 nm and two to three stacked layers, values similar to those inferred here [14]. Similarly, Khan et al. (2024) reported that thermal reduction consistently yields rGO with mixed structural order,

aligning with the ID/IG ratios observed in this study [15]. The absence of a well-defined 2D band, together with the presence of a weak second-order feature, is consistent with thermally reduced graphene oxide containing partially restored sp^2 domains and significant structural disorder.

The combination of techniques establishes that the material used in this study is rGO with partial restoration of its crystalline structure, but still containing functional groups essential for dispersion in NdFeB powders. These findings are critical because they validate the multifunctional role of rGO: (i) providing lubrication and dispersion during mechanical milling, (ii) forming a physical barrier to oxygen diffusion, and (iii) contributing to interfacial stabilization between NdFeB grains. Such multifunctionality is difficult to achieve with fully reduced or pristine graphene, which typically lacks sufficient chemical anchoring ability [26].

3.2 Effects of the mechanical milling parameters on the structure and microstructure of the NdFeB rGO composite

The incorporation of rGO during the mechanical milling of NdFeB powders produced significant changes in powder behavior, morphology, and structural stability. A central observation was the prevention of spontaneous ignition. NdFeB powders obtained by hydrogen decrepitation (HD) and milled without additives are known to ignite when exposed to air due to their high surface reactivity and affinity for oxygen [4]. In this study, however, NdFeB powders milled with 0.02 wt% rGO showed no signs of ignition when removed from the milling bowl, enabling safe handling in ambient atmosphere. This effect is attributed to rGO acting as a physical barrier and as a lubricant, preventing localized heating and minimizing surface energy during particle collisions [18]. The ability to process NdFeB powders in air without inert atmospheres or glove boxes represents an important breakthrough in powder metallurgy of rare-earth magnets, reducing both cost and complexity, as shown in Fig. 2a.

Transmission electron microscopy (TEM) confirmed the role of rGO in modifying powder morphology (Fig. 2b). Thin, stacked rGO flakes were observed encapsulating NdFeB particles, with two to three layers coating particle surfaces. The central particle core, with darker contrast, corresponded to the NdFeB alloy, while the lighter peripheral layers confirmed the presence of rGO. This encapsulation acts as a conformal shell, protecting particles from oxidation and stabilizing their surface chemistry. Similar rGO encapsulation has been reported in other composite systems, where graphene derivatives improved particle stability and dispersion [30, 31]. The encapsulation observed here reinforces the hypothesis that rGO can effectively mitigate surface reactions while remaining integrated into the microstructure of the final sintered magnet.

XRD patterns (Fig. 2c) of the milled powders confirmed the predominance of the $Nd_2Fe_{14}B$ phase (JCPDS 79-1994) with no detectable secondary oxides. This finding demonstrates that neither the milling process nor the addition of rGO altered the crystallographic integrity of the main magnetic phase. The preservation of the $Nd_2Fe_{14}B$ structure under milling conditions highlights the protective role of rGO and contrasts with reports of uncontrolled oxidation in unprotected NdFeB powders [24]. The absence of secondary phases also indicates that the small amount of rGO (0.02 wt%) was well distributed and did not disrupt the alloy lattice.

Particle size analysis (Fig. 2d) revealed a systematic decrease in average particle size with increasing milling time. NdFeB–rGO–1 (7 min) exhibited an average size of 4.8 μm, NdFeB–rGO–2 (15 min) 3.1 μm, NdFeB–rGO–3 (30 min) 2.4 μm, and NdFeB–rGO–4 (45 min) 1.7 μm. These results are consistent with previous studies showing that extended milling promotes particle refinement and grain size reduction, directly affecting sintering behavior and magnetic performance [2, 8]. Notably, the particle-size reduction observed here occurred without excessive cold welding or agglomeration, effects commonly reported for unprotected NdFeB powders. The presence of rGO likely reduced particle–particle adhesion during milling, acting as a solid lubricant as reported in earlier studies [16]. Particle-size values correspond to the mean FSSS particle size (μm), with variability across independently prepared triplicates expressed as mean ± standard deviation, which is appropriate for assessing experimental reproducibility and trend consistency in materials processing studies.

An additional benefit of particle refinement is its influence on sintering. Smaller particles provide higher surface area, enabling improved diffusion and densification during consolidation. This enhances both mechanical integrity and magnetic coupling between grains, contributing to higher coercivity and energy product in the final magnet [24]. The systematic decrease in particle size observed across the milling times in this study allowed for a clear correlation with the magnetic properties later discussed, particularly the balance between Br and iHc.

The prevention of ignition, combined with improved particle refinement and surface encapsulation, underscores the multifunctional role of rGO in NdFeB composites. Without rGO, handling NdFeB powders outside controlled environments is considered unsafe and often unfeasible for industrial-scale production. By mitigating these risks, rGO reduces dependence on expensive infrastructure such as glove boxes and inert gas systems, thus lowering operational costs and improving scalability [18]. Moreover, rGO-assisted processing provides intrinsic

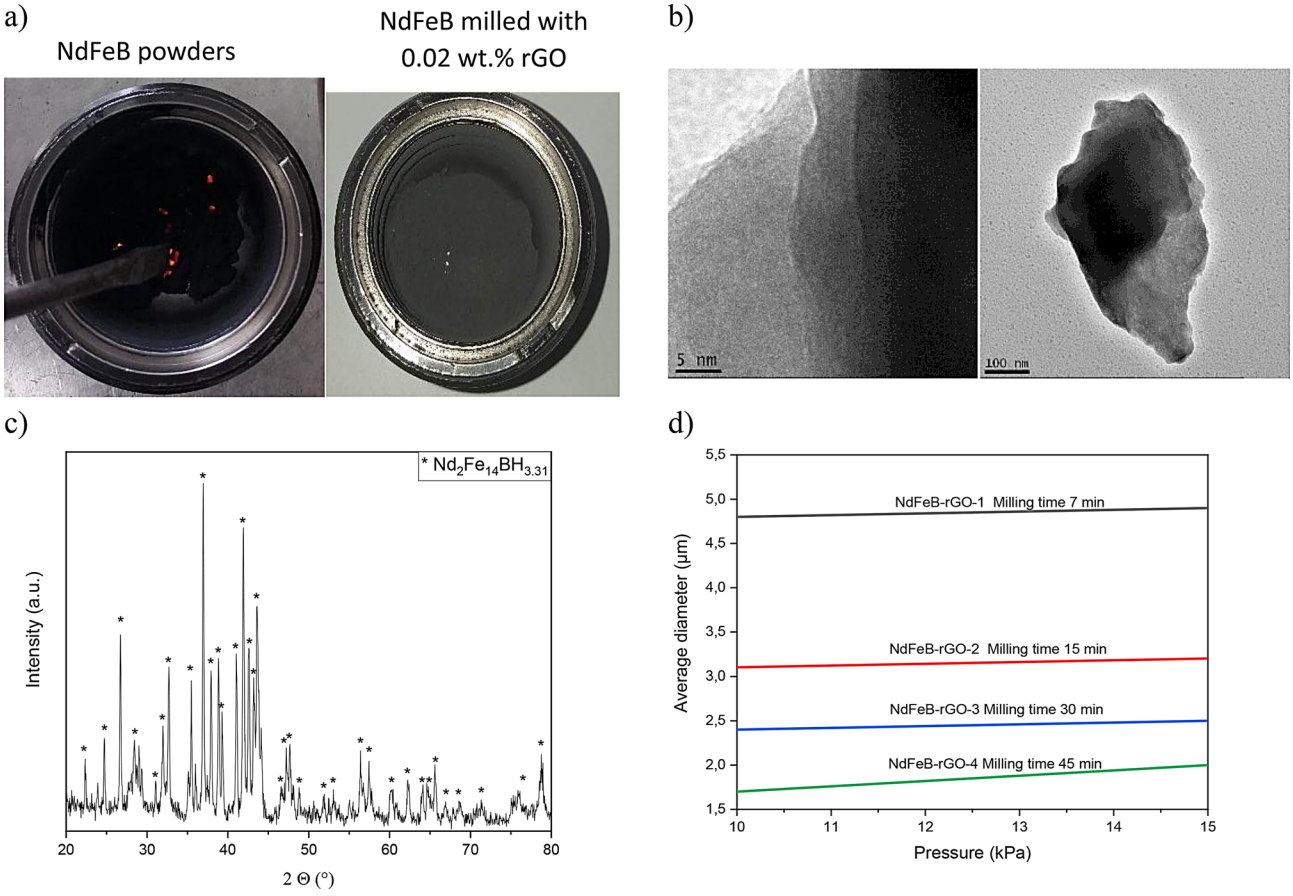

Fig. 2 Characterization of the NdFeB–rGO composite: (**a**) Photographs illustrating powder handling behavior under ambient air exposure: (i) pure NdFeB powder obtained by hydrogen decrepitation showing spontaneous ignition upon exposure to air, and (ii) NdFeB powder mechanically milled with 0.02 wt% rGO showing no ignition under identical handling and exposure conditions; (**b**) TEM image showing NdFeB particles surrounded by thin rGO sheets; (**c**) XRD pattern confirming the preservation of the $Nd_2Fe_{14}B$ phase after mechanical milling with rGO; (**d**) Mean particle size determined by Fisher Sub-Sieve Sizer (FSSS) as a function of mechanical milling time (7, 15, 30, and 45 min). Data correspond to the mean particle size (µm) obtained from independently prepared triplicate batches

oxidation resistance without relying on external coatings, which are typically required only after magnet fabrication. This represents a change in basic assumptions in processing methodology, aligning with efforts to improve sustainability and reduce environmental footprint in magnet production [26].

The observations in this study are consistent with the broader literature on graphene-modified composites. Similar lubrication and barrier effects of rGO have been reported in metallic and ceramic matrices, where rGO not only reduced processing defects but also enhanced corrosion and wear resistance [15]. However, this is one of the first studies to directly integrate rGO into the powder metallurgy of NdFeB magnets, offering both scientific novelty and practical implications.

3.3 Magnetic performance of sintered NdFeB–rGO magnets

The influence of rGO addition and milling duration on the magnetic properties of sintered NdFeB magnets was systematically investigated. In the Table 2 summarizes the main parameters: remanence (Br), intrinsic coercivity (iHc), and maximum energy product (BH_{max}). The results reveal a strong dependence on milling time, consistent with previous studies showing that microstructural refinement significantly affects magnetic performance [25].

Table 2 Magnetic properties of sintered NdFeB–rGO magnets as a function of milling time: remanence (Br), intrinsic coercivity (iHc), maximum energy product (BHmax), and squareness factor (SQ)

Sample	Br (T)	iHc (kAm^{-1})	BH_{max} ($kJ\ m^{-3}$)	SQ
Magnet-1	0.65	543.54	57.07	0.20
Magnet-2	0.81	454.10	74.42	0.25
Magnet-3	1.11	794.13	242.02	0.87
Magnet-4	1.02	765.07	181.25	0.53

The optimal balance between Br and iHc was obtained for Magnet-3 (30 min milling), yielding values comparable to commercial N35-grade magnets

Figure 3(a) presents the demagnetization curves for magnets produced with 0.02 wt% rGO and Fig. 3 (b) shows Raman spectroscopy of the magnets (Table. SI 1; Table. SI 2; Table. SI 3).

For Magnet-1, milled for 7 min, the values obtained were Br = 0.65 T, iHc = 543.5 kA·m^{-1}, and BH_{max} = 57.1 kJ·m^{-3}. These modest results reflect the relatively large particle size (~ 4.8 µm) and limited microstructural refinement. Compared to the optimized milling conditions (Magnets-3 and – 4), Magnet-1 exhibits the lowest remanence, which is attributed to insufficient particle refinement and densification, leading to weak intergranular exchange coupling and incomplete magnetic decoupling. As a result, magnetic performance is limited, particularly in terms of energy products. Similar trends have been reported for short milling durations in Fe- and Mn-based permanent magnets, where insufficient particle refinement results in reduced coercivity and remanence [32, 33].

Magnet-2, corresponding to 15 min of milling, showed improved Br = 0.81 T and moderate coercivity of 454.1 kA·m^{-1}, yielding BH_{max} = 74.4 kJ·m^{-3}. The increase in remanence suggests improved particle compaction and more effective interparticle contact during sintering. However, coercivity remained limited by incomplete refinement and the persistence of residual oxidation sites. This intermediate behavior indicates that, although milling was sufficient to reduce particle size (~ 3.1 µm), the microstructure was not yet optimized to maximize coercivity.

The most remarkable results were obtained for Magnet-3, milled for 30 min. This sample reached Br = 1.11 T, iHc = 794.1 kA·m^{-1}, and BHmax = 242.0 kJ·m^{-3}. These values are comparable to commercial N35-grade magnets and represent a favorable combination of remanence and coercivity. The strong squareness factor (SQ = 0.87) indicates efficient magnetic coupling and a relatively uniform microstructure. Grain refinement induced by 30 min of milling produced particles of ~ 2.4 µm, promoting dense packing and minimizing intergranular defects. The enhancement in coercivity is consistent with a grain-size-dependent hardening mechanism (Hall–Petch-like behavior), in which reduced grain size hinders domain wall motion [24]. At the same time, remanence remained high, indicating that excessive structural disorder was avoided. These findings highlight the critical balance between refinement and preservation of crystalline order achieved under this milling condition.

Extending the milling time to 45 min (Magnet-4) resulted in Br = 1.02 T, iHc = 765.0 kA·m^{-1}, and BH_{max} = 181.2 kJ·m^{-3}. Although coercivity remained high, remanence and energy products decreased compared to Magnet-3. This deterioration is attributed to excessive structural disorder, abnormal grain growth, and increased defect density, which impair effective long-range magnetic coupling. Similar behavior has been reported in the literature, where over-milling reduces the effective anisotropy field and introduces non-magnetic phases that lower Br and BH_{max} [8, 32, 33]. These results confirm that milling times beyond 30 min lead to diminishing returns and may degrade overall magnetic performance.

Raman spectroscopy provided complementary insights into the structural role of rGO in the magnets (Fig. 3b). All samples exhibited the characteristic D (~ 1350 cm^{-1}) and G (~ 1590 cm^{-1}) bands of carbon materials, confirming the partial retention of rGO after sintering. The persistence of rGO bands suggests that graphene derivatives

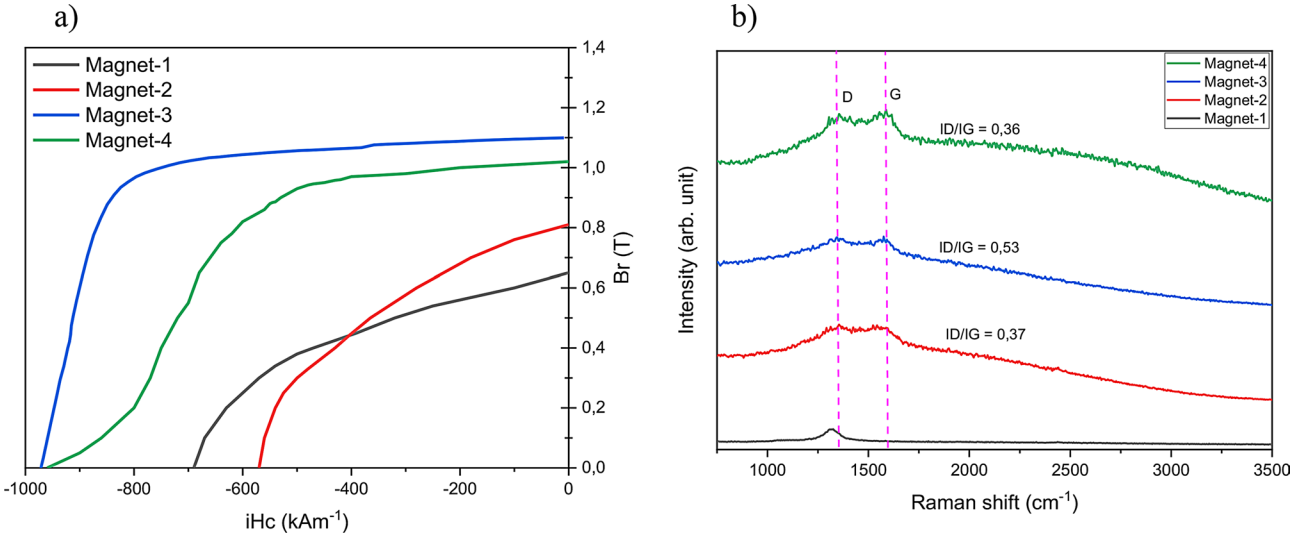

Fig. 3 Magnetic properties of sintered magnets with rGO: (**a**) Demagnetization curves comparing Magnet-1 to Magnet-4, showing the effect of milling time on remanence and coercivity; (**b**) Raman spectra of the magnets, with D and G bands confirming partial retention of rGO after sintering

were not fully consumed during consolidation and may contribute to microstructural stabilization. The variation in ID/IG ratio among samples indicates differences in disorder, which correlated with milling duration. Magnet-3 exhibited a balanced ID/IG ratio, consistent with partial preservation of graphitic domains, which may have facilitated both powder lubrication during milling and barrier formation during sintering [17].

The performance achieved in this study stands out when benchmarked against conventional processing routes. Lopes et al. (2012) showed that carbon impurities typically reduce coercivity in metal injection molding of NdFeB magnets [6]. However, the results here demonstrate that rGO, even as a carbonaceous additive, improved coercivity when adequately dispersed. Similarly, Xia et al. (2017) reported that recycling routes often suffer from poor coercivity due to oxidation, whereas the present work achieved values comparable to freshly sintered commercial magnets [13].

From a practical standpoint, the optimized condition (Magnet-3) suggests that rGO facilitates safe powder handling while simultaneously enhancing functional properties. The energy product (242 kJ·m^{-3}) aligns with targets for intermediate-performance magnets used in electronics and small motors. While higher-grade magnets for electric vehicles or wind turbines still require Dy/Tb additions for thermal stability, the approach demonstrated here offers a cost-effective route for producing stable magnets without heavy rare-earth elements. Furthermore, the ability to obtain strong magnetic performance under ambient processing conditions represents a significant technological advance, reducing reliance on inert atmospheres and complex safety protocols [18].

3.4 Corrosion resistance and surface degradation of NdFeB–rGO magnets

The electrochemical impedance spectroscopy (EIS) results provide important insights into the corrosion behavior of sintered NdFeB–rGO magnets in 3.5 wt% NaCl solution. Figure 4 shows the Bode magnitude and phase angle plots after immersion, comparing magnets processed with different milling times. Clear differences in electrochemical response were observed, confirming that rGO content and milling duration influence the passive behavior of the magnets.

Magnet-4 reached impedance values on the order of ~ 10^6 Ω, while Magnet-3 exhibited values around ~ 10^5 Ω, both significantly higher than those observed for Magnets-1 and – 2. These values represent up to two orders of magnitude improvement compared to impedance moduli typically reported for conventionally coated NdFeB magnets in similar NaCl electrolytes [13, 34].

In contrast, Magnets-1 and – 2 showed lower impedance moduli and broader impedance responses, with multiple relaxation processes, indicative of less stable passive layers. These results demonstrate that both milling duration and optimized rGO encapsulation play a key role in enhancing interfacial stability and corrosion resistance, even in the absence of external protective coatings.

For clarity, the comparison expressed as "two orders of magnitude" refers to low-frequency impedance modulus values (|Z|) reported in the literature for NdFeB magnets protected by conventional surface coatings, such as Ni–P or diamond-like carbon (DLC) layers, tested in similar NaCl electrolytes [13, 34]. In those systems, typical impedance modulus values are commonly reported in the range of 10^4 Ω, whereas the rGO-assisted magnets

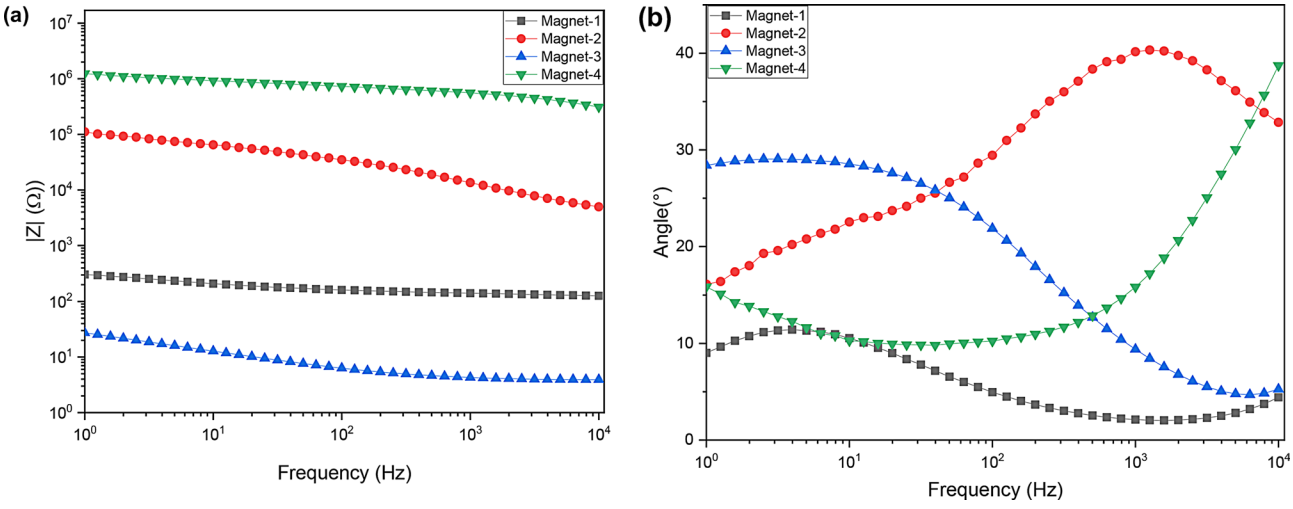

Fig. 4 Electrochemical impedance spectroscopy in 3.5 wt% NaCl solution for sintered NdFeB–rGO magnets: (**a**) Bode magnitude plots showing up to two orders of magnitude improvement in low-frequency impedance modulus, particularly for Magnet-4, compared to values typically reported for conventionally coated NdFeB magnets in similar electrolytes; (**b**) Bode phase plots indicative of the formation of stable passive interfacial layers in Magnets-3 and – 4

investigated here exhibit values on the order of 10^6 Ω under comparable electrochemical conditions. This comparison is literature-based and intended to provide contextual benchmarking rather than a direct experimental comparison or circuit-model fitting.

Consistent with the impedance magnitude results, the phase angle plots further highlight differences among the samples. Magnet-4 exhibited a response close to a single-time-constant behavior, which is indicative of a relatively stable and compact interfacial barrier at the electrode–electrolyte interface. Such behavior is commonly associated with systems of low electrochemical activity and effective hindrance of ionic transport [35]. Magnet-3, although displaying slightly lower impedance modulus than Magnet-4, still maintained high impedance values on the order of 10^5 Ω and a well-defined phase angle maximum. This response is consistent with the presence of an effective protective interfacial layer, albeit less blocking than that observed for Magnet-4. Overall, these results suggest that intermediate to long milling times promote improved rGO distribution and densification, leading to enhanced interfacial stability and superior corrosion resistance relative to shorter milling conditions.

Enhanced corrosion behavior can be attributed to several mechanisms. First, the encapsulation of NdFeB particles by rGO sheets, observed in TEM analyses, likely contributes to surface passivation by physically blocking oxygen and chloride ion diffusion. Graphene-based materials are nearly impermeable to gases and electrolytes, and even partially reduced rGO can act as an effective barrier [17]. Second, particle size refinement promoted by milling increased compactness and reduced porosity, decreasing pathways for electrolyte penetration. Similar correlations between densification and improved corrosion resistance in NdFeB magnets have been reported by Li et al. (2022) [36]. Third, the presence of residual oxygen groups in rGO may facilitate interfacial bonding with metallic surfaces, stabilizing passive layers and reducing localized corrosion [28].

Wu et al. (2017) reported impedance values around 10^4 Ω for NdFeB magnets coated with diamond-like carbon films, while the present rGO-assisted samples achieved 10^6 Ω without coatings [12]. Zhao et al. (2024) demonstrated that Ni–P–GO–Y coatings improved wear and corrosion resistance, but such multilayer coatings add complexity and cost. By contrast, the results here indicate that incorporating rGO directly into the powder during milling provides intrinsic protection, eliminating the need for post-processing coatings [12, 34]. This not only reduces manufacturing steps but also ensures protection throughout the bulk of the material, rather than relying on a surface film that may delaminate during service.

It is important to note, however, that the observed differences between Magnet-3 and Magnet-4 highlight the need to optimize milling duration. While both exhibited excellent corrosion resistance, the magnetic performance of Magnet-3 was superior, with higher BH_{max} and remanence. Excessive milling (45 min) produced higher impedance values but compromised magnetic properties, likely due to structural disorder and excess carbon accumulation at surfaces. These results indicate that intermediate milling time (30 min) provides the best balance between corrosion resistance and magnetic performance, whereas prolonged milling favors corrosion stability at the expense of magnetization.

The implications of these findings are significant for the development of NdFeB magnets. By eliminating the need for protective coatings, rGO-assisted processing reduces both production costs and environmental impact. Coating processes often involve toxic chemicals, additional equipment, and generate waste, whereas the direct use of rGO during milling simplifies processing. Moreover, the observed improvement of two orders of magnitude in impedance modulus compared to coated references demonstrates that this approach provides long-term durability suitable for demanding applications such as electric motors and wind turbines.

3.5 Surface chemistry depth profiling by RBS

Surface chemistry and microstructure play decisive roles in the performance of NdFeB magnets, particularly in balancing corrosion resistance and magnetic stability. In this study, Rutherford Backscattering Spectrometry (RBS) and field emission scanning electron microscopy (FESEM) were used to evaluate the effects of rGO incorporation and milling time on the elemental distribution and morphology of the sintered magnets.

Figure 5 (a and b) shows depth profiles of carbon and oxygen obtained by RBS for magnets processed under different milling durations (Fig S3). A general trend was observed: both carbon and oxygen concentrations decreased with depth, confirming that surface contamination and oxidation are localized to the outermost layers. For Magnet-1 (7 min), oxygen started at ~ 36 wt% near 125 nm depth and dropped to ~ 20 wt% in the bulk. Carbon levels were also elevated at the surface, reflecting exposure to air and incomplete encapsulation. These features are consistent with the lower corrosion resistance measured by EIS and the relatively poor magnetic performance of this sample, highlighting the susceptibility of insufficiently milled powders to oxidation [37, 38].

In contrast, Magnet-3 (30 min) exhibited a distinct profile. Surface oxygen content reached ~ 40 wt% at ~ 100 nm but decreased rapidly to ~ 21 wt% with depth, forming a thin and stable passive layer. Carbon content was lower than in other samples, ~ 17 wt% at the surface, and dropped below 5% deeper into the material. This reduced carbon concentration is beneficial, as excess carbon at

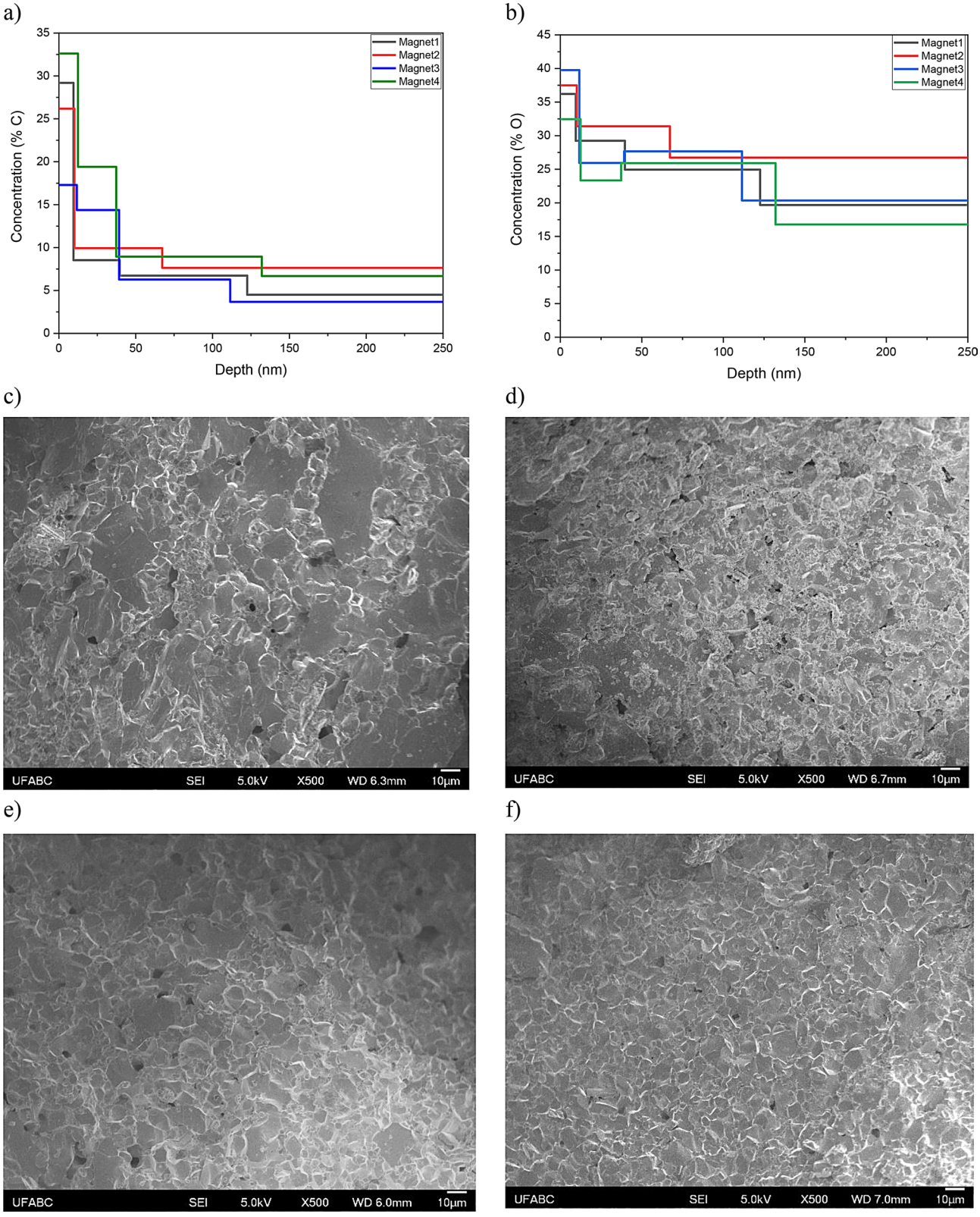

Fig. 5 Surface and microstructural analyses of sintered magnets with rGO: (**a**) Carbon depth profiles obtained by RBS, indicating surface accumulation dependent on milling time; (**b**) Oxygen depth profiles, evidencing the formation of protective passive layers; (**c**) and (**d**) FESEM images of Magnet-1 and Magnet-2, showing heterogeneous microstructures; (**d**) and (**f**) FESEM images of Magnet-3 and Magnet-4, showing more homogeneous and compact grains

grain boundaries is known to impair magnetic coupling and decrease coercivity [6, 7]. The combination of a thin oxygen-rich layer and limited carbon accumulation likely explains why Magnet-3 achieved the best balance of corrosion resistance and magnetic properties.

Magnet-4 (45 min) showed higher surface carbon (~ 33 wt%) compared to Magnet-3, although oxygen profiles were similar. The excess carbon is attributed to longer milling time, which increases surface activation and promotes carbon uptake from rGO and the environment. While this contributed to slightly improved corrosion resistance, as indicated by higher impedance in EIS, it compromised remanence and energy product. This trade-off underscores the importance of optimizing rGO distribution and milling parameters to avoid excess non-magnetic carbon phases at the surface [8, 32].

These RBS findings corroborate surface-sensitive XPS results, which identified mixtures of metallic and oxidized states for Nd, Fe, and Co in the composites (SI. 2 Results). The agreement between XPS (surface chemistry) and RBS (depth-resolved composition) provides robust evidence that rGO contributes to surface stabilization, but the degree of protection depends strongly on milling duration. Similar depth gradients of oxygen and carbon have been reported in NdFeB alloys exposed to air, but the presence of rGO here clearly modulated these profiles, reducing uncontrolled oxidation and stabilizing interfaces [23].

Morphological analysis by FESEM (Fig. 5c–f) highlights clear differences in grain evolution among the samples. Magnet-1 and Magnet-2 exhibit heterogeneous microstructures, characterized by a wide dispersion of grain sizes and irregular particle morphologies, consistent with insufficient milling and less effective compaction.

In Magnet-3, the micrographs suggest a comparatively more homogeneous and densely packed microstructure, with finer grains and reduced porosity relative to the shorter milling conditions. Although a full quantitative grain-size distribution is beyond the scope of the present work, such refinement and densification are commonly associated with improved sintering behavior in NdFeB systems, particularly when particle size is reduced and surface chemistry is modified [2, 5].

Magnet-4 exhibited irregular morphologies including locally refined grains relative to the intermediate milling conditions, indicating heterogeneous refinement and localized structural disorder. These features suggest that excessive milling introduces stress and defects that interfere with controlled grain growth. As a result, although Magnet-4 exhibits high coercivity, it shows reduced remanence and BHmax, a trend widely reported in over-milled permanent magnets where structural disorder degrades magnetic anisotropy and exchange interactions [6, 39]. It should be emphasized that the FESEM observations provide qualitative insight into microstructural heterogeneity, and no quantitative definition of a "normal" grain size is implied in this discussion.

The combined FESEM and RBS analyses indicate that Magnet-3 achieves a balanced microstructural and surface condition. Its limited carbon incorporation and stabilized oxygen-containing surface layer promote corrosion resistance while preserving effective grain-boundary exchange interactions, which are known to be essential for achieving high remanence and coercivity in NdFeB magnets [2, 5].

Compared with literature approaches based on external coatings, such as silanes or Ni–P alloys [11], the present strategy introduces rGO during milling, providing intrinsic stabilization distributed throughout the microstructure. This internal protection acts before, during, and after sintering, reducing dependence on post-processing treatments and potentially lowering production cost and environmental impact.

Moreover, the results highlight the multifunctional role of rGO. Beyond its barrier properties, rGO appears to facilitate densification, suppress excessive oxidation, and modulate grain size distribution. This multifunctionality is particularly valuable in NdFeB systems, where the simultaneous optimization of corrosion resistance and magnetic performance is challenging. The superior properties of Magnet-3 underscore that precise control of milling parameters and rGO content can unlock synergies unattainable with conventional methods.

The combined results from structural, magnetic, electrochemical, and surface analyses highlight the multifunctional role of rGO as an additive in NdFeB magnet processing. By comparing the performance of powders and sintered magnets across different milling durations, it becomes clear that rGO acts simultaneously as a protective, dispersive, and structural stabilizing agent, and that optimal properties emerge when milling time is carefully controlled.

The prevention of spontaneous ignition in rGO-containing powders is a major advance for safe processing. Conventional NdFeB powders are highly reactive and ignite in air, requiring glove boxes or inert atmospheres [4]. In this work, rGO effectively prevented ignition, enabling ambient handling and reducing infrastructure costs. TEM confirmed that this behavior results from rGO encapsulation, which forms thin protective layers around NdFeB particles. Such protection not only improves safety but also suppresses uncontrolled surface oxidation, creating more favorable conditions for subsequent sintering [35].

Magnetic results reinforced this interpretation. Milling for 30 min produced Magnet-3, which combined high remanence (1.11 T), coercivity (794 $kA{\cdot}m^{-1}$), and maximum energy product (242 $kJ{\cdot}m^{-3}$). These values approach

those of commercial N35 magnets, despite the absence of Dy or Tb additions. The balance between Br and iHc at this condition demonstrates that moderate milling achieves sufficient grain refinement without introducing excessive disorder [24, 25]. Longer milling (45 min) further increased surface protection but degraded magnetic properties due to structural defects and carbon accumulation, while shorter times (7–15 min) yielded incomplete refinement. These trends confirm that milling time is a critical variable for optimizing NdFeB–rGO composites.

Electrochemical analysis provided complementary evidence. EIS revealed that Magnets-3 and – 4 exhibited impedance values of ~ 10^6 Ω, surpassing the ~ 10^4 Ω typically reported for coated NdFeB magnets [12, 34]. This two-order-of-magnitude improvement was achieved without external coatings, demonstrating that rGO incorporation during milling intrinsically enhances corrosion resistance. The formation of a thin oxygen-rich passivation layer, combined with dense microstructures and reduced porosity, accounts for the improved stability [26, 36].

RBS and FESEM results further explained the surface–microstructure relationship. Magnet-3 exhibited low surface carbon (~17 wt%) and high oxygen (~40 wt%), indicative of a stable passivation layer. FESEM confirmed a homogeneous grain distribution, correlating with superior coercivity and remanence. In contrast, Magnet-4 accumulated excess surface carbon (~33 wt%), which reduced magnetic coupling despite high corrosion resistance. These results show that optimal performance arises not from maximizing corrosion protection alone, but from balancing surface chemistry and microstructural stability [8, 40].

The novelty of this approach lies in integrating rGO directly during powder processing, rather than applying coatings after sintering. External coatings, such as Ni–P or DLC, provide temporary protection but are prone to delamination and mechanical failure [7, 23]. By contrast, rGO distributes throughout the powder and microstructure, ensuring intrinsic protection and scalability. Furthermore, the method eliminates the need for controlled atmospheres, reduces reliance on heavy rare-earths, and lowers environmental impact compared to conventional protective strategies.

4 Conclusions

The incorporation of 0.02 wt% rGO during the mechanical milling of NdFeB alloys proved to be an effective approach to overcome key limitations of conventional processing. The additive enabled safe handling of powders under ambient conditions, eliminating the need for inert atmospheres or glove boxes and thus improving industrial feasibility and reducing production costs. Structural analyses confirmed the multifunctional role of rGO, acting as both a solid lubricant and an encapsulating agent. This dual behavior prevented spontaneous ignition, reduced surface oxidation, and stabilized particle chemistry during milling and sintering. Milling time was shown to be critical: short times yielded insufficient refinement, while prolonged times led to structural disorder and carbon accumulation.

At the intermediate milling time of 30 min, the magnets achieved the best performance, with high remanence (1.11 T), robust coercivity (794 $kA{\cdot}m^{-1}$), and a competitive maximum energy product (242 $kJ{\cdot}m^{-3}$). Electrochemical impedance spectroscopy further revealed corrosion resistance two orders of magnitude higher than conventional systems, without the need for surface coatings. Overall, these results highlight rGO as a multifunctional additive for safer, more sustainable, and scalable production of high-performance NdFeB permanent magnets.

Supplementary Information

The online version contains supplementary material available at https://doi.org/10.1007/s44308-026-00014-5.

Supplementary Material 1

Acknowledgements

CNPQ project: 400872/2019-6 and 142164/2020-8 process. INCT Project: CNPQ (465719 / 2014-7), FAPESP (2014 / 50887-4) and CAPES (23038000776/2017-54), the Materials Science and Technology Center (CCTM/IPEN), Laboratory of Electrical Engineering (POLI/USP), the National Graphite and IPEN-CNEN/SP. CNPq (444303/2018-9)), FINEP and FAPESP (CEPID - CDMF 2013/07296-2). Research supported by CTI's Open Labs – Multiple Users and Shared Facilities, CTI Renato Archer, research institution from MCTI. The Multiuser Laboratory of Functional Polymers and Surface Engineering the UFABC and, research used resources of the Laboratory of Material Analysis with Ion Beams - LAMFI-USP, of the University of São Paulo. The author(s) acknowledge the laboratory staff for assistance during the experiments.

Author contributions

Silva-Filho: Conceptualization, Writing—Original Draft, Writing, Review & Editing, Funding acquisition. Carvalho da Silva: Investigation, writing, formal analysis. Takiishi: Conceptualization, Investigation, Formal analysis. Mazon: Writing, Review & Editing. Venancio: Investigation. Rangel: Formal analysis. Abe: Formal analysis. Janasi: Investigation, Formal analysis. Meira: Formal Analysis. Romero: Formal analysis. Fiorini da Silva: Formal Analysis. Lima-Rodrigues: Formal Analysis. Guimaraes: Writing, Review & Editing. Freelon: Writing, Review & Editing. Antunes: Formal analysis, Writing, Review & Editing. Martinez: Formal analysis. Escote: Formal analysis, Writing Review & Editing. Rey: Investigation, Formal analysis.

Funding

CNPQ project: 400872/2019-6 and 142164/2020-8 process.

Data availability

All data generated or analyzed during this study are included in this published article.

Declarations

Competing interests

The authors declare no competing interests.

Received: 16 October 2025 / Accepted: 23 February 2026
Published online: 27 February 2026

References

1. Prasad Mishra T, Leich L, Krengel M, Weber S, Röttger A, Bram M. NdFeB Magnets with well-pronounced anisotropic magnetic properties made by electric current-assisted sintering. Adv Eng Mater. 2023;25(1):2201027. https://doi.org/10.1002/adem.202201027.
2. Cui J, Kramer M, Zhou L, Liu F, Gabay A, Hadjipanayis G, Sellmyer GD. Current progress and future challenges in rare-earth-free permanent magnets. Acta Mater. 2018;158:118–37. https://doi.org/10.1016/j.actamat.2018.07.049.
3. Ghorbani Y, Ilankoon IMSK, Dushyantha N, Nwaila GT. Rare earth permanent magnets for the green energy transition: Bottlenecks, current developments and cleaner production solutions. Resour Conserv Recycl. 2025;212:107966. https://doi.org/10.1016/j.resconrec.2024.107966.
4. Gielen D, Lyons M. Critical materials for the energy transition: Rare earth elements. International Renewable Energy Agency; 2022. pp. 1–48.
5. Renquan W, Ying L, Jun L, Linhua C, Xiaojiao Y, Yuchong Q. Effect of crushing methods on morphology and magnetic properties of anisotropic NdFeB powders. J Rare Earths. 2017;35(8):800–4. https://doi.org/10.1016/S1002-0721(17)60979-7.
6. Takiishi H, Lima L F C P, Costa I, Faria RN. The influence of process parameters and alloy structure on the magnetic properties of NdDyFeBNb HD sintered magnets. J Mater Process Technol. 2014;152(1):1–8. https://doi.org/10.1016/j.jmatprotec.2003.10.022.
7. Lopes L, Carvalho M, Chaves RS, Trevisan MP, Wendhausen PA, Takiishi H. Study of carbon influence on magnetic properties of metal injection molding Nd-Fe-B based magnets. Mater Sci Forum. 2012;727:124–9. https://doi.org/10.4028/www.scientific.net/MSF.727-728.124.
8. Fim RGT, Silva MRM, Silva SC, Casini JCS, Wendhausen PAP, Takiishi H. Influence of Milling Time on Magnetic Properties and Microstructure of Sintered Nd-Fe-B Based Permanent Magnets. Mater Sci Forum. 2018;930:445–8. https://doi.org/10.4028/www.scientific.net/MSF.930.445. Trans Tech Publications Ltd.
9. Cao XJ, Chen L, Guo S, Li XB, Yi PP, Yan AR, Yan GL. Coercivity enhancement of sintered Nd–Fe–B magnets by efficiently diffusing DyF3 based on electrophoretic deposition. J Alloys Compd. 2015;631:315–20. https://doi.org/10.1016/j.jallcom.2015.01.078.
10. Fu J, Wang D, Gao Y, Yu H, Zhu D, Song Y, Liu G. Microstructure and super-high coercivity of Tb-containing NdFeB magnets by diffusion with Tb metal and Pr-Al-Cu-Ga. AIP Adv. 2025;15(7). https://doi.org/10.1063/5.0273816.
11. Chen J, Yang H, Xu G, Zhang P, Lv J, Sun W, Wu Y. Phosphating passivation of vacuum evaporated Al/NdFeB magnets boosting high anti-corrosion performances. Surf Coat Technol. 2020;399:126115. https://doi.org/10.1016/j.surfcoat.2020.126115.
12. Wu H, Xiao S, Chen D, Qasim AM, Ding K, Wu G, Chu PK. Effects of diamond-like carbon film on the corrosion behavior of NdFeB permanent magnet. Surf Coat Technol. 2017;312:66–74. https://doi.org/10.1016/j.surfcoat.2016.09.008.
13. Xia M, Abrahamsen AB, Bahl CR, Veluri B, Søegaard AI, Bøjsøe P. Hydrogen decrepitation press-less process recycling of NdFeB sintered magnets. J Magn Magn Mater. 2017;441:55–61. https://doi.org/10.1016/j.jmmm.2017.01.049.
14. Silva Filho JC, Venancio EC, Silva SC, Takiishi H, Martinez LG, Antunes RA. A thermal method for obtention of 2 to 3 reduced graphene oxide layers from graphene oxide. SN Appl Sci. 2020;2(8):1–8. https://doi.org/10.1007/s42452-020-03241-9.
15. Khan A, Sapakal SN, Kadam A. Comparative analysis of graphene oxide (GO) reduction methods: impact on crystallographic, morphological, and optical properties. Graphene and 2D Materials. 2024:1–9. https://doi.org/10.1007/s41127-024-00072-y.
16. Silva-Filho JC, Silva SC, Fim RGT, Takiishi H. Preparation of magnetic, ferrous, and non-ferrous powders, using rGO, GO and G as milling agents. Brazilian National Institute of Industrial Property; 2019. (BR. Patent no10 2019 016267 8).
17. Chadha N, Sharma R, Saini P. A new insight into the structural modulation of graphene oxide upon chemical reduction probed by Raman spectroscopy and X-ray diffraction. Carbon Lett. 2021;1–7. https://doi.org/10.1007/s42823-021-00234-5.
18. Filho JS, Silva SC, Takiishi H, Janasi SR, Martinez LG, Rey JFQ, Escote MT. A New Method of Neodymium-Iron-Boron Magnets/Reduced Graphene Oxide Manufacturing Without a Controlled Atmosphere. JOM. 2024;76(6):3073–80. https://doi.org/10.1007/s11837-024-06525-2.
19. James RW. D-Ray Crystallography. John Willy and Sons Inc; 1961.
20. Cullity BD. Elements of X-Ray Diffraction. Addison-Wesley Publishing Company, Inc. 1956.
21. Mayer M. Improved physics in SIMNRA 7. Nucl Instrum Methods Phys Res Sect B. 2014;v 332:p176–80. https://doi.org/10.1016/j.nimb.2014.02.056.
22. Silva TF, Rodrigues CL, Mayer M, Moro MV, Trindade GF, Aguirre FR, Tabacniks MH. (2016) MultiSIMNRA: A computational tool for self-consistent ion beam analysis using SIMNRA. Nuclear Instruments and Methods in Physics Research Section B: Beam Interactions with Materials and Atoms, 371, 86–9. https://doi.org/10.1016/j.nimb.2015.10.038.
23. Silva TF, Rodrigues CL, Added N, Rizzutto MA, Tabacniks MH, Höschen T, Mayer M. Self-consistent ion beam analysis: An approach by multi-objective optimization. Nucl Instrum Methods Phys Res Sect B. 2021;506:32–40. https://doi.org/10.1016/j.nimb.2021.09.007.
24. Dirba I, Aravindhan A, Muneeb M, Gutfleisch O. Grain size and coercivity tuning in Nd2Fe14B-based magnets prepared by high pressure hydrogen milling. J Magn Magn Mater. 2023;582:171018. https://doi.org/10.1016/j.jmmm.2023.171018.
25. Younes A, Amraoui R, Bouamer A, Guessoum M, Boutaghou Z, Smaili F, Mendoud A. Effect of milling time on the structural and magnetic properties of nanostructured Fe. 2024. https://doi.org/10.1007/s11664-024-11252-0.
26. Pozenel Kovacic T, Kovacevic N, Milosev I. Corrosion of Sintered NdFeB Permanent Magnets. J Electrochem Soc DOI. 2025. https://doi.org/10.1149/1945-7111/ade509.
27. Popescu AM, Calderon-Moreno JM, Yanushkevish K, Aplevich A, Demidenko O, Neacsu EI, Constantin V. Corrosion Behavior of NdFeB Magnets in Different Aqueous Solutions. J Braz Chem Soc. 2024;35:e–20230089. https://doi.org/10.21577/0103-5053.20230089.
28. Al-Gaashani R, Najjar A, Zakaria Y, Mansour S, Atieh MA. XPS and structural studies of hig quality graphene oxide and reduced graphene oxide prepared by different chemical oxidation methods. Ceram Int. 2019;45(11):14439–48. https://doi.org/10.1016/j.ceramint.2019.04.165.
29. Qiu Y, Guo F, Hurt R, Külaots I. Explosive thermal reduction of graphene oxide-based materials: mechanism and safety implications. Carbon. 2014;72:215–23. https://doi.org/10.1016/j.carbon.2014.02.005.
30. Adam RE, Chalangar E, Pirhashemi M, Pozina G, Liu X, Palisaitis J, Nur O. Graphene-based plasmonic nanocomposites for highly enhanced solar-driven photocatalytic activities. RSC Adv. 2019;9(52):30585–98. https://doi.org/10.1039/C9RA06273D.
31. Chang S, Zhang Q, Lu Y, Wu S, Wang W. High-efficiency and selective adsorption of organic pollutants by magnetic CoFe2O4/graphene oxide adsorbents: Experimental and molecular dynamics simulation study. Sep Purif Technol. 2020;238:116400. https://doi.org/10.1016/j.seppur.2019.116400.
32. Patel K, Zhang J, Ren S. Rare-earth-free high energy product manganese-based magnetic materials. Nanoscale. 2018;10(25):11701–18. https://doi.org/10.1039/C8NR01847B.
33. Liang D, Zhu T, Shao Z, Liu S, Han J, Du H, Yang J. Study on the relationship between structure and magnetic properties of τ-phase MnAl prepared by cryo-milling. AIP Adv. 2024;14(1). https://doi.org/10.1063/9.0000642.
34. Godavarthi S, Porcayo-Calderon J, Vazquez-Velez E, Casales-Diaz M, Ortega-Toledo DM, Martinez-Gomez L. Influence of the chemical composition in the electrochemical response of permanent magnets. J Spectrosc. 2015. https://doi.org/10.1155/2015/356027.
35. Calabrese L, Capri A, Fabiano F, Bonaccorsi L, Borsellino C, Proverbio E. Corrosion behaviour of a silane protective coating for NdFeB magnets in dentistry. Int J Corros. 2015. https://doi.org/10.1155/2015/345038.
36. Li J, Yao Q, Huang W, Xie J, Mo Z, Deng J, Zhou H. Improvement in magnetic properties, corrosion resistance and microstructure of Nd–Fe–B sintered magnets through intergranular addition of Tb68Ni32. J Rare Earths. 2022;40(5):784–91. https://doi.org/10.1016/j.jre.2021.03.007.
37. Jeynes C, Barradas NP, Szilágyi E. Accurate determination of quantity of material in thin films by Rutherford backscattering spectrometry. Anal chem. 2012;84(14):6061–9. https://doi.org/10.1021/ac300904c.
38. Colaux JL, Jeynes C. High accuracy traceable Rutherford backscattering spectrometry of ion implanted samples. Anal Method. 2014:6(1):120–129. https://doi.org/10.1039/C3AY41398E.
39. Duan P, Ping Q, Sun D, Luo Q, Li H, Xu H, Du L. Electronic structures and magnetic properties of the rare-earth-free permanent magnet α′′-Fe 16 N 2: first-principles calculations. J Mater Chem C. 2025;13(13):6728–35. https://doi.org/10.1039/D4TC04934A.

40. Momeni V, Luca S, Gonzalez-Gutierrez J, Cano S, Sueur E, Shahroodi Z, et al. Binder System Composition on the Rheological and Magnetic Properties of Nd-Fe-B Feedstocks for Metal Injection Molding. Appl Sci. 2024;14(13):5638. . https://doi.org/10.3390/app14135638

Publisher's note